International Communications in Heat and Mass Transfer 158 (2024) 107946

Contents lists available at ScienceDirect

International Communications in Heat and Mass Transfer

journal homepage: www.elsevier.com/locate/ichmt

Comparison of heat transfer from single- and double-sided heated horizontal plate under free convection in air with constant heat flux condition

Michał Ryms [a,*], Krzysztof Tesch [b], Witold s.M. Lewandowski [a]

[a] Faculty of Chemistry, Department of Energy Conversion and Storage, Gdańsk University of Technology, Narutowicza 11/12, Gdansk 80-233, Poland
[b] Faculty of Mechanical Engineering and Ship Technology, Gdańsk University of Technology, Narutowicza 11/12, Gdansk 80-233, Poland

ARTICLE INFO

Keywords:
Free convective heat transfer
Horizontal plate
Double-sided heating
Experimental study
Balance method

ABSTRACT

This paper presents the results of an experimental and numerical study of convective heat transfer from a newly designed double-sided heated horizontal plate in air. To ensure equal heat transfer from both surfaces, the plate was equipped with two independently supplied electric heaters and resistance thermometers on each side. Minimizing the plate's thickness reduced lateral heat loss and improved measurement accuracy.

The study used the balance method for convective heat transfer analysis, and results were validated through standard numerical calculations for q = const. Additionally, results were compared with experimental literature for intermediate cases, such as a cuboid, where convection occurs from both horizontal and vertical sides.

Experimental results for the plate showed a 15.5–18.0% difference from numerical ones and a 24.7–29.3% difference from average extreme cases. These findings, presented as the Nusselt-Rayleigh relationship, were positively verified by numerical calculations, confirming their reliability. This advancement enables separate studies of free convection from the upper and lower parts of horizontal plates.

1. Introduction

Free convection in an open space appears to be a very well-studied case of heat transfer, especially from flat vertical, horizontal and diagonal surfaces [1–12], cylinders [13–21,22], cuboids [23–30] and other solids of complex shapes [31–34]. In the real conditions however, it turns out that this may not be entirely truth. For example, the results of free convection tests from flat horizontal surfaces with the heating surface pointing upwards or downwards differ depending on whether these surfaces are part of a horizontal plate or a cuboid.

For a typical horizontal Type I plate (heated on one side), the type of convective heat transfer depends on its orientation, either with the heated side up [3,4,35,36,37] or down [5,8], which can only be tested separately. On the other hand, in the case of a Type II plate heated on both sides and cuboids, convection occurs simultaneously from all theirs surfaces (Fig. 1a). In the case of an isothermal cuboid, as described in [25] and [27], the structure of the flow and the shapes of the boundary layer are transformed as the motion develops: as shown in Fig. 1b the horizontal flow of fluid (below the bottom), through a vertical flow past the side walls, there is a change in the direction of fluid motion to the horizontal over the lateral surface of the cuboid above which a convective free stream (plume) forms. This complex heat transfer mechanism is accompanied by the interaction of phenomena occurring on each surface, which does not happen in the case of unilaterally heated plates.

Analysis of the reasons for the discrepancies in the experimental results of free convection from horizontal plates and cuboids should also take into account another possible reason for their occurrence, namely, the accuracy of the calculated heating energy balance. In the case of a cuboid, all of the delivered and measured heating energy is transferred to the fluid, whereas in the case of a unilaterally heated horizontal plate of type I (the situation where the plate is heating one side only), the reverse and lateral heat loss flux Q_{loss} must be subtracted from the delivered heat flux. Therefore, for a unilaterally heated plate, the accuracy of the results depends strictly on how this flux is eliminated and estimated.

Although the concept of a thin double-sided heated plate was the subject of papers [38] and [7] (for constant wall temperature – CWT and under constant heat flux - CHF condition, respectively), both studies were based solely on numerical investigations. The aim and novelty of

* Corresponding author.
E-mail address: michal.ryms@pg.edu.pl (M. Ryms).

https://doi.org/10.1016/j.icheatmasstransfer.2024.107946

Available online 21 August 2024

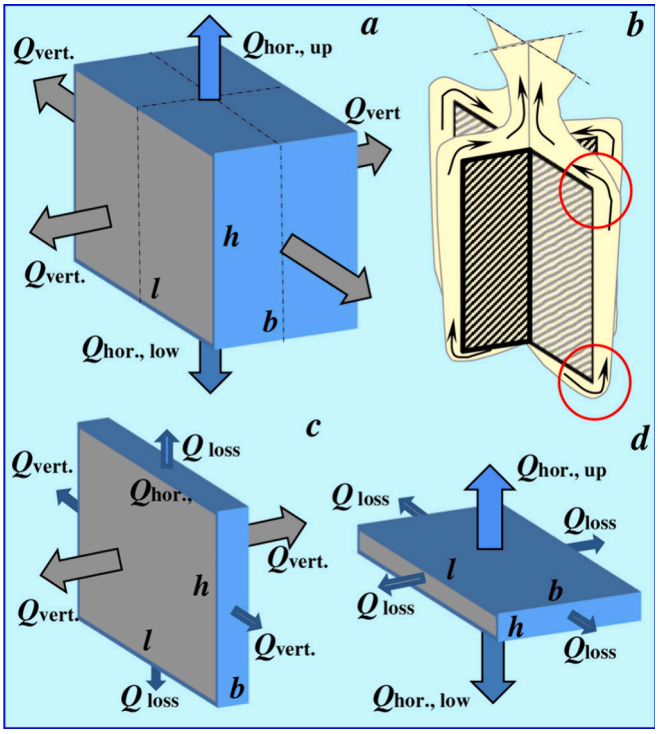

Fig. 1. An illustrative comparison of the contributions of the convective heat fluxes Qhor.,i, Qvert.,i and the heat loss fluxes Qloss,i of different shapes: a) cuboid, c) vertical plate, d) horizontal plate, b) the vertical transverse and longitudinal cross-sections of the convective boundary layers formed on the surface of a cuboid.

this study was to construct and test a newly designed horizontal double-sided heated plate (called Type II) with minimal thickness to limit heat loss from its side edges. This allows simultaneous testing of convective heat transfer from its upper and lower heating surfaces, which also increases the measurement accuracy of the balance method, as it is no longer necessary to subtract the reverse heat loss flow from the supplied heat flux. As the heat flux from this plate is entirely transferred to the fluid under test, as in the case with cuboids and cylinders, spheres and other heating solids, the planned verification of the results was based mainly on the results of tests of these configurations. Moreover, the double-sided heated plated (Type II) used in this work is so thin (2.1 mm) that it does not require its sides to be insulated with thermal insulation, without which the lateral heat loss (included in the energy balance), is negligible at only 4.2%.

2. Experimental background

2.1. Theoretical considerations

The intensity of convective heat transfer intensity, described by the Nusselt-Rayleigh relationship

$$\mathrm{Nu} = C{\cdot}\mathrm{Ra}^{n} \tag{1}$$

in which

$$\mathrm{Nu} = \frac{\alpha \bullet l_{ch}}{\lambda} = \frac{q \bullet l_{ch}}{\lambda \bullet (T_w - T_\infty)} = \frac{Q \bullet l_{ch}}{A \bullet \lambda \bullet (T_w - T_\infty)} \tag{2}$$

and

$$\mathrm{Ra} = \frac{g \bullet \beta \bullet (T_w - T_\infty) l_{ch}^{n}}{\nu \bullet a} \tag{3}$$

depends on the components of these numbers, i.e. the temperature difference between the heating surface and the undisturbed area $\Delta T = T_w - T_\infty$, the size of the heat transfer surface, expressed by the characteristic linear dimension l_{ch}, the physical properties of the medium (λ, β, ν, a) at the temperature of the phenomenon, conventionally taken to be $T_{av} = (T_w - T_\infty)/2$, and the heat transfer coefficient α and exponent n.

The heat transfer coefficient α from a heating element of any shape, such as a cuboid, plate, sphere, cylinder, cone, etc. (for which the methods of calculating the average α_{total} are given in the works [7,23,24,26,29,31,32,30], is related to the heat transfer rate by Newton's law:

$$Q = \alpha_{total} \bullet A \bullet (T_w - T_\infty) \tag{4}$$

For the cuboid, which is the optimum shape for experimental studies and theoretical considerations of convective heat transfer from the point of view of analogy with the horizontal and vertical planar plate, which are its characteristic cases, the value of the equivalent (total) heat transfer coefficient, which enables the Nusselt number to be determined, is described by the relationship:

$$\alpha_{total} = \frac{Q}{A \bullet (T_w - T_\infty)} \tag{5}$$

in which, in the case of electrical heating, the convective heat rate Q is equal to:

$$Q = U \bullet I - Q_{loss} \tag{6}$$

To determine α, in addition to measuring the voltage U and the supply current I, it is also necessary to know the heat loss flux to the surroundings Q_{loss}. In the case of the cuboid illustrated in Fig. 1.a, no heat loss flux occurs $Q_{loss} = 0$, because all the energy from it, after neglecting the energy losses through the supply lines and the slide, is entirely transferred convectively to the surroundings in the form of fluxes $Q_{hor,up}$, $Q_{hor,low}$ and $\sum Q_{vert,i}$.

Thus, the accuracy of the balance method for a cuboid, in the absence of heat loss, is high, as it depends only on the accuracy of the heating power meters, and on temperature and surface area measurements.

This certainty and high accuracy are important advantages of using this method in technical applications. However, from a scientific point of view, it is less useful, especially for the study of mechanisms and local phenomena in convective heat transfer, but it does work well for the verification of results obtained numerically [7,39,14], theoretically [24–26] or experimentally [27] using other methods, e.g. a local gradient method based on measuring the temperature gradient in the direction perpendicular to the heating surface.

Fig. 1b shows that convective flow patterns are transformed as the configuration of the perpendicular surface changes. Under its horizontal lower surface, a horizontal boundary layer forms, which then splits into four, pair-symmetrical, vertical boundary layers, which flow over the horizontal upper surface and over its centre merge to form a single vertical convection chimney (plume).

Thus, in the case of a cuboid, three contributions of convective heat transfer can be distinguished: one that is the vertical surfaces (Fig. 1c) and two others from the horizontal surfaces (upper and lower) (Fig. 1d).

However, in contrast to the cuboid, for which heat loss did not occur ($Q_{loss} = 0$), the heat loss fluxes ($Q_{loss} \neq 0$) for the separately considered vertical or horizontal heating plates, which are transferred to the surroundings from the horizontal edges of the vertical plate (Fig. 1c) or from the vertical edges of the horizontal plate (Fig. 1d), must also be taken into account.

These fluxes, which are difficult to measure or estimate disturb the fluid flow in the boundary layers, especially at the points marked by circles in Fig. 1b where the convective fluxes change direction. Consequently, this can affect the local and final boundary layer thicknesses δ and thus, according to the relation:

$$\alpha = \frac{\lambda}{\delta} \tag{7}$$

reduce the accuracy of the determination of the local heat transfer coefficient α.

The magnitude of the heat fluxes, and therefore also the heat losses, depends, according to (4), on the size of the lateral surface of the heating plate A_{loss}. Thus, when its thickness decreases then its lateral surface area also decreases ($A_{loss} \rightarrow 0$) and thus also the heat loss ($Q_{loss} \rightarrow 0$). What is less obvious is that heat loss also depends on the position of the plate itself. If it is positioned vertically, heat loss occurs only from its horizontal sides $A_{loss,\ vert.} = 2{\cdot}l{\cdot}b$, whereas in a horizontal orientation the vertical peripheral side surface of this plate is greater and is $A_{loss,\ hor.} = 2{\cdot}(l + b){\cdot}h$. Since these surfaces are not equal ($Q_{loss,vert.} \neq Q_{loss,hor.}$), as can be seen more clearly in Fig. 1, the heat loss from the plate in the horizontal position is also slightly greater.

These differences are due to the fact that, for a vertical plate, the two surfaces of the side edges are also vertical and exchange heat in the same way as the side heating surfaces of the heating plate, according to the mechanism of free convection heat transfer from a vertical surface. In this situation, heat loss $Q_{loss,vert.}$ Occurs only from the two surfaces of the horizontal edges of the plate (upper and lower) $A_{loss,vert.} = 2{\cdot}l{\cdot}b$ (Fig. 1. c). However, for a horizontal plate perpendicular to its heating surfaces (upper and lower) the heat loss area is greater and is $A_{loss,hor.} = 2{\cdot}(l + b){\cdot}h$ (Fig. 1d).

For example, for the thinnest experimental plate we were able to make with two internal heaters and two external resistance thermometers with dimensions 0.150, 0.075 and 0.0021 m [1], the heat loss areas are $A_{loss,vert} = 2{\cdot}l{\cdot}b = 0.00063\ m^2$ and $A_{loss,hor.} = 2{\cdot}\ (l + b){\cdot}h = 0.000945\ m^2$. For T_w = const the proportions of the loss fluxes Q_{loss} to the convective heat fluxes Q in the case of the vertical position, with heating area $A_{vert.} = 2{\cdot}h{\cdot}(l + b) = 0.022815\ m^2$, are $Q_{loss}/Q_{vert.} = 0.0276$ while for the horizontal orientation, with area $A_{hor.} = 2{\cdot}l{\cdot}b = 0.0225\ m^2$, they are higher and reach approx. $Q_{loss}/Q_{hor.} = 0.042$.

The study of this plate, carried out in a vertical configuration (Fig. 1c) and assuming bilateral symmetry of convective heat transfer in air, confirmed that, by reducing its thickness to $b = 0.0021$ m, it was indeed possible to reduce the heat loss flux to about 3% in relation to the convective fluxes studied and thus increase the accuracy of the balance method. The results obtained and their reliability made it possible to demonstrate the hypothetical possibility of temperature duality of the Rayleigh number in free convection [2].

Current research focuses on carrying out a similar but much more difficult experimental study of convective heat transfer in air using the same plate, but in a horizontal configuration, which would increase the proportion of heat loss to about 4.2% compared to a vertical plate and further exclude the possibility of using the symmetry condition of the phenomenon, which in the case of a vertical plate allowed the assumption $N/2 = Q_{left} = Q_{right}$.

2.2. Construction of the heating plate

A heating plate with minimised heat losses and thus increased accuracy of the individual measurement of heat fluxes from both heating sides is the most important element of the free convection test using the balance method. The heating plate used in this research, with dimensions $l = 150$ mm, $b = 75$ mm and $h = 2.1$ mm, is improved version (0.9 mm thinner) of the plate described in paper [1]. It consists of three layers: a single copper-coated laminate LAM100X160H0.6 of 0.6 mm thickness with lithographically etched paths of the upper surface resistance thermometer to measure $T_{w,up}$ (Fig. 2a), two sides of a copper-coated LAM100X160ED0.6 0.6 mm thick with two etched electrical resistance heaters (N_{up}, N_{low}) (Fig. 2b) and again from a single copper-coated laminate LAM100X160H0.6 with etched lower resistance thermometer paths to measure $T_{w,low}$ (mirror image Fig. 2a).

These elements were glued together under pressure with epoxy resin. During the bonding process, Kevlar braided fishing line was attached to the shorter edges of the plate. Thermal bridges were thus avoided by

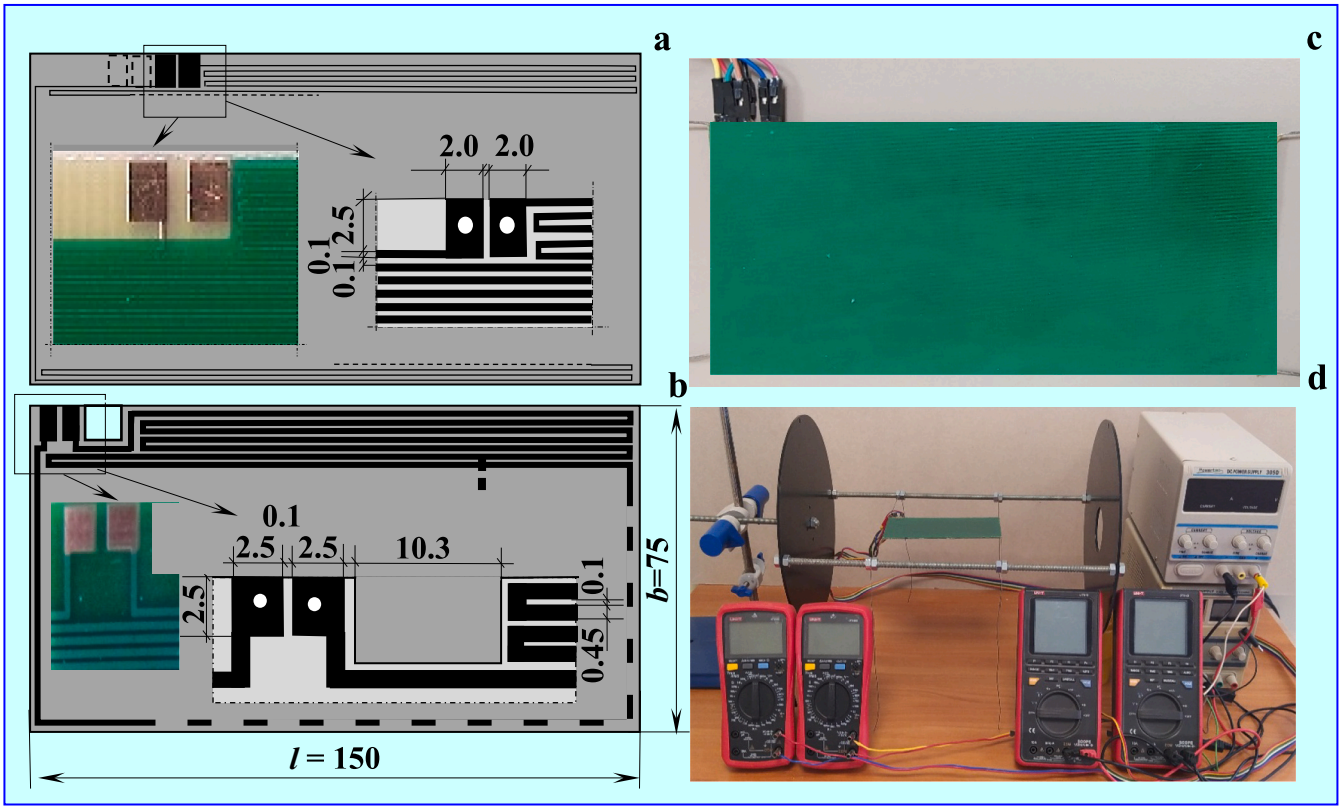

Fig. 2. Design drawings of the etched paths in the three heating plate components, with enlarged portions: a) one-sided copper-clad (two resistance thermometers), b) two-sided copper-clad (two-sided heater), c) view of the completed plate, d) view of the test bench without shields.

fixing the plate in the test bench (Fig. 2d) in this way, without the aid of metal brackets or slides.

2.2.1. Heaters

The design of the heaters was preceded by power calculations. For the assumption that the experimental tests will be carried out for convective heat transfer in the laminar range ($Ra \leq 10^7$), in air λ (50 °C) = 0.0283 W/(m·K), $\Delta T_{max} = 50$ K, for plate dimensions $l = 0.15$ and $b = 0.075$ m and assuming $Nu = 0.71 \cdot Ra^{1/4}$ [3–5], the convective heat rate transferred to air, determined from Eq. (3), is:

$$Q = \alpha \bullet A \bullet \Delta T_{max} = \frac{Nu \bullet \lambda \bullet A \bullet \Delta T_{max}}{l} = 0.71 \bullet Ra^{\frac{1}{4}} \bullet \lambda \bullet b \bullet \Delta T_{max}$$
$$= 0.71 \bullet \left(10^7\right)^{\frac{1}{4}} \bullet 0.0283 \bullet 0.075 \bullet 50 = 4.24 \text{ W} \quad (8)$$

After taking into account the convective heat loss flux from one heater $Q_{loss} \approx 4.2/2\%$ and the radiation flux, in this case also the heat loss, $Q_{rad.} \approx 1.5 \cdot Q_{conv.}$, the optimum power of one heater is obtained:

$$N_{heaters} = U \bullet I = Q = 4.24 \bullet 1.021 \bullet (1 + 1.5) = 10.82 \text{ W} \quad (9)$$

To power these heaters, it was decided to use two single DC power supplies of $N = 30$ W, voltage $U = 0$–30 V and current $I = 0$–3 A, or one dual power supply.

For the three current voltages $U = 10$, 20 and 30 V, the resistance of the heater, calculated from the relation:

$$R = \frac{U^2}{N_{heaters}} \ \Omega \quad (10)$$

would be $R = 9.24$ Ω (for 10 V), 36.96 Ω (for 20 V) and 83.16 Ω (for 30 V). It was decided to design a heater with an average of the above three heater resistances $R \approx 43$ Ω, but before taking the final decision, a check was made to ensure that the corresponding current resistance was within the operating range of the power supply:

$$I = \sqrt{\frac{N_{heaters}}{R}} = \sqrt{\frac{10.82}{43.0}} = 0.50 \text{ A} \quad (11)$$

and that the current did not exceed the maximum allowable current that could melt or burn out the heater paths.

The maximum current for a path of width determined by the successive approximation method $b_{Cu} = 0.45$ mm, etched in copper with a thickness of $g_{Cu} = 18$ μm and a rectangular cross-section $F = 0.45 \times 0.018 = 0.0081$ mm^2, corresponding to a conductor cross-section of diameter $d = 0.10$ mm, is $I_{max} = 2.75$ A [9].

This check was successful, so for the assumed resistance and path width, the matrix for the exposure and photolithographic etching of the heaters on both sides was LAM100X160ED0.6 of thickness 0.6 mm, made from epoxy resin reinforced with fibre- glass, double-sided with a copper layer of thickness 18 μm. With the minimum feasible spacing between the paths $s = 0.1$ mm and path width $b_{Cu} = 0.45$ mm, the calculated length of each of the heaters, covering the entire upper and lower surfaces of the plate evenly with the coils (see enlarged section in Fig. 2b), was 19.88 m.

After taking into account this length, the cross-sectional area and the specific resistance of the copper $\rho = 1.68 \cdot 10^{-8}$ Ω (at 0 °C) and $\rho = 1.72 \cdot 10^{-8}$ Ω (at 20 °C) the resistance of the heater was calculated:

$$R = \rho \frac{l}{F} = 1.68 \bullet 10^{-8} \bullet \frac{19.88}{0.018 \bullet 10^{-3} \bullet 0.45 \bullet 10^{-3}}$$
$$= 41.2 \left(0^0\text{C}\right), 42.2 \left(20^0\text{C}\right) \Omega \quad (12)$$

From a dozen or so etched laminate plates, the one whose resistances on both sides were most similar to each other was chosen to build the heating plate. These resistances measured at room temperature, of $R_{up} = 42.9$ Ω and $R_{low} = 43.0$ Ω, differed by only +1.6 and + 1.9% from those designed and calculated from Eq. (12).

2.2.2. Resistance thermometers

Resistance thermometers etched in copper covering on one side the epoxy laminate reinforced with glass fibre are an analogue of the Pt100 thermistor with a resistance of 100 Ω made from platinum wire. The sensitivity of a resistance thermometer depends on the measurement accuracy of the resistance $R_t - R_0$ and the resistance of the thermometer at temperature R_0. For the assumed accuracy of measurement $R_t - R_0 = 0.1$ Ω, the resistance at the reference temperature $R_0 = 100$ Ω and the temperature resistance coefficient α ($\alpha_{Cu} = 3.9 \cdot 10^{-3}$ K^{-1}), the sensitivity is:

$$\text{Sensitivity} = \frac{R_t - R_0}{\alpha \bullet R_0} = \frac{0.1}{3.9^{-3} \bullet 100} = 0.26 \text{ K} \quad (13)$$

As can be seen from Eq. (12), the sensitivity of the thermometer depends on R_0, so at the design stage it was decided to obtain the highest possible resistance of the thermometers etched in copper, at which their sensitivity should also be high.

Since the maximum resistance allowed by the LAM100X160E0.6 laminate with a copper layer thickness of $g_{Cu} = 0.035$ mm was already obtained in the thermometers used in earlier research [1], it was decided in the present work to use the LAM100X160H0.6 laminate with the thinnest of manufactured coatings $g_{Cu} = 0.018$ mm.

With the narrowest path of width $s = 0.1$ mm, obtained in a copper coating of thickness $g_{Cu} = 0.018$ mm when making the heaters using the etching technique, and an assumed minimum distance between paths, also $b_{Cu} = 0.1$ mm, a thermometer 56.26 m long should theoretically be formed on the surface of the plate. The shape of its cross-section may depend on the depth of etching and may change from rectangular for thin copper layers to trapezoidal for thick ones.

If we have a uniform distribution of paths of width $b_{Cu} = 0.1$ mm and a spacing $s = 0.1$ mm (enlarged section in Fig. 2a), after taking into account the specific resistance of the copper $\rho_{Cu} = 1.68 \cdot 10^{-8}$ Ω (0 °C) and $\rho_{Cu} = 1.72 \cdot 10^{-8}$ Ω (20 °C) and assuming a rectangular cross-section of paths, the theoretical resistance of the thermometer should be:

$$R = 1.68 \bullet 10^{-8} \bullet \frac{56.26}{0.1 \bullet 10^{-3} \bullet 0.018 \bullet 10^{-3}} = 525.1 \ (0^oC),$$
$$= 537.6(20^oC) \ \Omega \quad (14)$$

As with the etching of the heaters, a dozen thermometers were also made in an attempt to keep the exposure and etching times of the plates the same. Those thermometers with the highest resistance were chosen in the first step, from which, in turn, the two with the most similar resistances were selected: $R_{up} = 408$ Ω and $R_{low} = 398$ Ω. The resistance of the thermometers selected to build the hot plate is approximately 4 times higher than that of the Pt100, which, according to Eq. (13), translates into an increase in their sensitivity to 0.06 K.

3. Experimental study

3.1. Calibrating the resistance thermometers of the heating plate

In the horizontal position with different free convective mechanisms and heat fluxes on the upper and lower heating surfaces, the results of a calibration carried out for the whole plate would be unreliable. The calibration was therefore carried out with the heating plate in the vertical position, in the knowledge that the heat fluxes from both its surfaces were the same.

3.2. Experimental investigation of a horizontal plate in air

The study of convective heat transfer from an isothermal horizontal surface in air was carried out in the standard way. For a given heating power, which was the same for the upper and lower surfaces, $N_{up} = N_{low} = I_{up}U_{up} = I_{low}U_{low}$, after thermodynamic equilibrium was established, i.e. constant temperatures $T_{w,uper}$ = const and $T_{w,low}$ = const and the

averaged ambient temperature T_∞ = const, the results were recorded, i.e. $T_{w,up}$, $T_{w,low}$, T_∞, I_{up}, U_{up}, I_{low}, U_{low}. Thereafter, the measurement for the next set power was started.

The ambient temperature was measured with thermocouples at a distance of 1.5 m from the plate at three levels: - 0.5 m, 0 m (plate level) and + 0.5 m. In order to counteract air movements disrupting convective heat transfer in a multifunctional and continuously operated laboratory, the test bench was isolated with a shield of a shape similar to that shown in Fig. 3. The dimensions of this shield, made from plaster board of thickness g = 10 mm, did not coincide with those adopted for the numerical calculations: height H = 1.6 m, width B = 1.0 m and length L = 1.2 m.

Because of the method of heating, with resistive heaters distributed evenly over the upper and lower surfaces in the form of a single etched copper path, it is very likely that the UHF (Uniform Heat Flux) condition is met. Fulfilment of this condition is more realistic than in the case of heating with the resistive foil that is usually used for this purpose. The parallel flow of current through the foil, which depends on local variations in its thickness, can cause local overheating. This does not happen when a series current flows through the resistive path.

The surface resistance thermometers make it possible to measure accurately, with a resolution of 0.06 K, but only the average surface temperatures $T_{w,up}$ and $T_{w,low}$. It should be noted, however, that case, where $T_{w,up} = T_{w,low}$, does not prove that the CWT_{total} (Constant Wall Temperature) condition is satisfied for both sides of the heated plate.

In contrast, the entire surface of the horizontal plate used in this study, heated by two surface resistance heaters, can theoretically satisfy CHF condition. It is expected that occurrence of such situation will be shown by the results of experimental tests carried out using the balance method and by the results of numerical calculations.

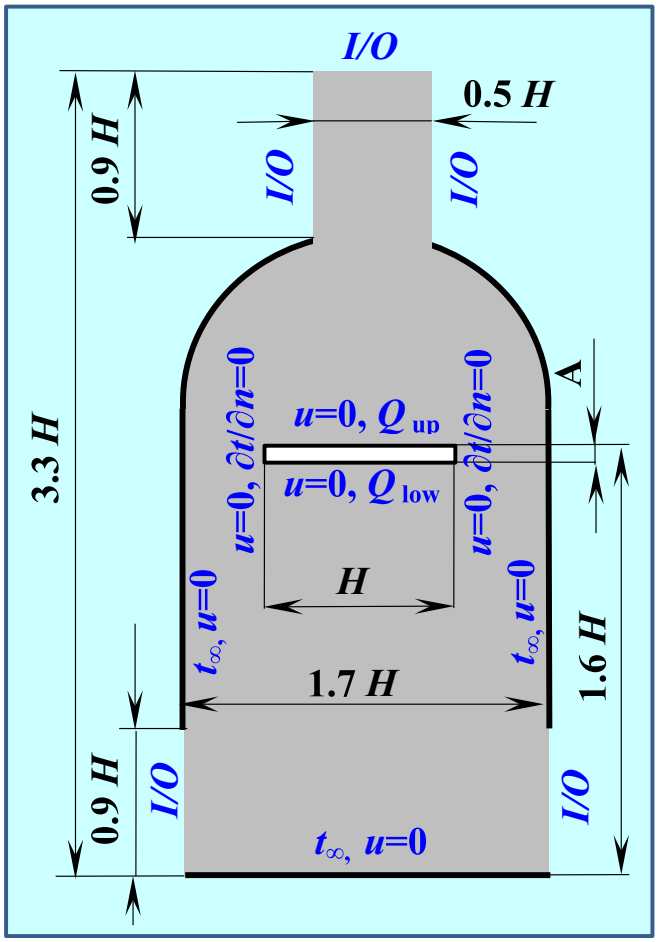

Fig. 3. Flow domain with boundary conditions.

Theoretically, it is possible to carry out convective heat exchange with a double-sided heated plate of plate tests, taken as a whole, by heating them with the same heat flux (CHF). In this work, it was decided to set the same heating powers of the upper and lower surfaces of the plate ($Q_{up} = Q_{low}$ = const.) for each measurement point and, once the thermodynamic equilibrium was established, to measure $T_{w,up}$ and $T_{w,low}$. In both cases the Nusselt numbers can be calculated using the relationships:

$$\mathrm{Nu} = \frac{Q \bullet b}{\lambda \bullet A \bullet (T_w - T_\infty)}, \mathrm{Nu}_{up/low} = \frac{Q_{up/low}}{\lambda \bullet l \bullet (T_w - T_\infty)}, \mathrm{Nu}_{total} = \frac{Q_{total}}{\lambda \bullet 2 \bullet l \bullet (T_w - T_\infty)} \tag{15}$$

To calculate the Rayleigh numbers for the plate, Eq. (3) was used, taking b as the characteristic linear dimension and the exponent $n = {}^1/_5$, which, according to the majority of authors quoted in Table 4, better describes the convective heat transfer to horizontal surfaces than n = ¼, used for vertical surfaces.

In the case of $q = Q/A$ = const, the Rayleigh numbers were calculated from the equation:

$$\mathrm{Ra}^* = \mathrm{Ra} \bullet \mathrm{Nu} = \frac{g \bullet \beta \bullet Q b^4}{A \bullet \lambda \bullet \nu \bullet a}, \mathrm{Ra}^*_{up/low} = \frac{g \bullet \beta \bullet Q_{up/low} \bullet b^3}{l \bullet \lambda \bullet \nu \bullet a} \text{ and } \mathrm{Ra}^*_{total} = \frac{g \bullet \beta \bullet Q_{total} \bullet b^3}{2 \bullet l \bullet \lambda \bullet \nu \bullet a} \tag{16}$$

The following formulae describing the values of the physical properties of air (λ, β, $\nu = \mu/\rho$ and $a = \lambda/(c_p\rho)$) (18)–(21) as a function of the mean temperature t_{av} expressed in Kelvin were used to determine the Nusselt and Rayleigh numbers:

$$\beta = 1/T_{av}\ 1/\mathrm{K} \tag{17}$$

$$\rho = 101,300\ [\mathrm{Pa}]/(287.1\ [\mathrm{J/(mol\cdot K)}]\cdot T_{av})\ \mathrm{kg/m^3} \tag{18}$$

$$\lambda = -3.5723023\cdot10^{-4} + 1.2587814\cdot10^{-4}\cdot T_{av} - 2.6237125\cdot10^{-6}\cdot {T_{av}}^{1.5} + 2.5229349\cdot10^{-8}\cdot {T_{av}}^2\ \mathrm{W/(m\cdot K)} \tag{19}$$

$$\mu = (-5.375\cdot10^{-1} + 1.811\cdot10^{-2}\cdot T_{av} + 11.41\cdot ln(T_{av}) + 1.330\cdot10^4/{T_{av}}^{1.5} - 6.800\cdot10^4/{T_{av}}^2)\cdot10^{-6}\ \mathrm{kg/(m\cdot s)} \tag{20}$$

$$c_p = 6.3869\cdot10^2 + 0.4032\cdot T_{av} + 1.9951\cdot10^5/T_{av} - 29,124\cdot10^6/{T_{av}}^{1.5} + 1.2788\cdot10^7/{T_{av}}^2\ \mathrm{kJ/(kg\cdot K)} \tag{21}$$

The convective heat flux in Eq. (15) is not only related to the heat energy transferred from the heater, but also takes into account the heat loss through radiation Q_{rad} and convection from the side edges of the plate, were estimated to be Q_{loss} = 2.1% for the upper and lower surfaces or Q_{loss} = 4.2% for whole plate:

$$Q = N - Q_{rad} - Q_{loss} = U \bullet I \bullet 0.958 - Q_{rad} \tag{22}$$

where:

$$Q_{rad} = A \bullet \sigma \bullet \varepsilon \bullet (T_w^4 - T_\infty^4) \tag{23}$$

and $\sigma = 5.67\cdot10^{-8}$ W/(m^2·K^4) and ε = 0.884 [1].

3.3. Numerical calculations

Apart from verifying the results of the experimental studies carried out using the balance method, the numerical studies aimed to compare the results of convective heat transfer from a bilaterally heated

horizontal plate assuming CHF condition.

Steady-state solutions were obtained by means of transient CFD calculations performed in order to verify the results of the experimental study. A compressible turbulent airflow without the Boussinesq approximation was considered. The closed system of equations consists of the mass conservation equation:

$$\frac{\partial \rho}{\partial \tau} + \nabla \bullet (\rho \mathbf{u}) = 0 \tag{24}$$

the Navier-Stokes equation

$$\frac{\partial (\rho \boldsymbol{u})}{\partial \tau} + \nabla \bullet (\rho \mathbf{u}\mathbf{u}) = -\nabla p_{rgh} - (\boldsymbol{g} \bullet \boldsymbol{r}) \nabla \rho + \nabla \bullet (2\mu \boldsymbol{D}) - \nabla \left(\frac{2}{3} \mu \nabla \bullet \boldsymbol{u} \right) \tag{25}$$

the thermal equation of state

$$p = \rho R T \tag{26}$$

$$\frac{\partial (\rho (h + K))}{\partial \tau} + \nabla \bullet (\rho \mathbf{u}(h + K)) = \frac{\partial \mathrm{p}}{\partial \tau} + \nabla \bullet (\alpha \nabla h) + \rho \boldsymbol{u} \bullet \boldsymbol{g} \tag{27}$$

and the enthalpy equation, where the modified pressure p_{rgh}, the gravity acceleration vector $\boldsymbol{g}$, the position vector $\boldsymbol{r}$, the strain rate tensor $2\boldsymbol{D}$ and the macroscopic kinetic energy K are:

$$p_{rgh} = p - \rho \boldsymbol{g} \bullet \boldsymbol{r}, \boldsymbol{g} = -g\boldsymbol{j}, \boldsymbol{r} = -y\boldsymbol{j}, 2\boldsymbol{D} = \nabla \boldsymbol{u} + (\nabla \boldsymbol{u})^T, K = \frac{1}{2} \|\boldsymbol{u}\|^2 \tag{28}$$

Furthermore, the discretised system of equations was solved directly using the Finite Volume Method [40]. Free convection was therefore solved as transient, until the pseudo-steady state was reached, which took up to 25 s, depending on the wall temperature. Moreover, the discretised system of equations was solved by means of the PISO algorithm [41], where the pressure equation was solved using the GAMG algorithm. In order to calculate the velocity and enthalpy, preconditioned bi-conjugate gradient solvers together with diagonal-based incomplete lower upper (DILU) solvers were utilised. The discretised convection terms were interpolated by means of linear upwind interpolation, and the discretised Laplacian terms involving surface normal gradients made use of orthogonal schemes. The gradients also involved Gaussian integration and linear interpolation. The fluxes were based on linear interpolation. The flow domain together with the boundary conditions is shown in Fig. 3. In order to minimise the impact of the environment on the results, the test bench was enclosed, which is accurately reflected in the shape of the computational domain and the boundary conditions. The horizontal plate is bounded on the sides by screens to minimise the impact of the surroundings. The no-slip condition was applied to the walls of the plates, screens and the bottom surface along with the pressure gradient established in such a way that the boundary flux follows the velocity boundary condition.

Several surfaces such as the upper and lower sides were regarded as an inlet/outlet (I/O) in order to ensure air circulation. By I/O conditions are meant the mixed-type velocity boundary conditions, i.e. for the inflow, the velocity was calculated from the face normal component of the internal-cell value and for the outflow a zero-gradient condition was specified. On the upper and lower walls of the plates, the Neumann condition was established in the form of a known power Q, while the lateral surfaces of the plates were treated as adiabatic, i.e. the zero Neumann condition. The constant values of other parameters adopted for the calculations were $c_{\mathrm{p}} = 1004$ J/kg/K, Pr = 0.705 and $\mu = 1.831 \cdot 10^{-5}$ kg/m/s.

The flow domain was discretised using a Cartesian mesh with a carefully selected number of nodes.

The effect of the number of nodes on the average temperatures of the plates is shown in Fig. 4 a). It can be seen from that increasing the number of nodes beyond $3 \cdot 10^5$ does not further alter the results in terms of average temperatures. Therefore, a calculation mesh with a node count of $3 \cdot 9 \cdot 10^5$ was selected for further calculations. The maximum y^+ values on the plate walls did not exceed 0.15. An example of the calculation mesh and example results from the numerical simulation are shown in Fig. 5.

Fig. 4 b) shows the effect of time step on the results. In the range of time steps considered, it can be seen that their choice does not affect the average temperatures. In contrast, longer time steps would be associated with a loss of stability in the calculations. On the basis of the above analysis, a time step of 0.005 s was selected, as decreasing it further does not improve the results, and such a value guaranteed stability for the entire series of calculations.

4. Results

4.1. Results of experimental studies of a horizontal plate

The experimental studies of free convection from a horizontal plate in air could be carried out by simultaneously increasing the heating power of both heaters by the same values, i.e. from the point of view of the plate achieving the constant power condition of the CHF heat fluxes. For each surface of this upper and lower plate, considered separately. The results obtained for free convection heat transfer from a double-sided horizontal heating plate, referred to as type II, to air are shown graphically in Fig. 6.

As the experiments were carried out for three heating modes of the plate, they have been marked in the figures as follows: black circles when each heating element (upper and lower) was heated independently with two power supplies (i), blue diamonds when the heating elements were connected in series (s) and red squares when they were connected in parallel with one power supply (p). For each of these heating modes, up to two selected example test points are given in Table 1, for which, in addition to the measured parameters, the calculation results are also given.

From the experimental results carried out for the whole plate, shown

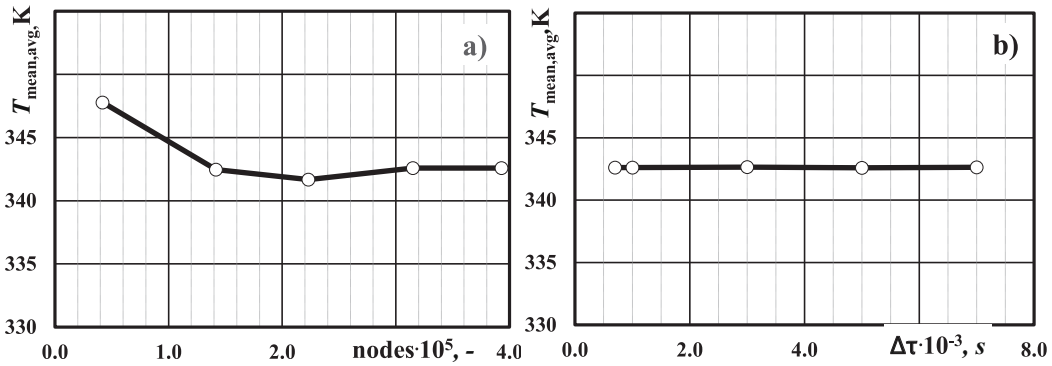

Fig. 4. Impact of a) mesh size, b) time step on results.

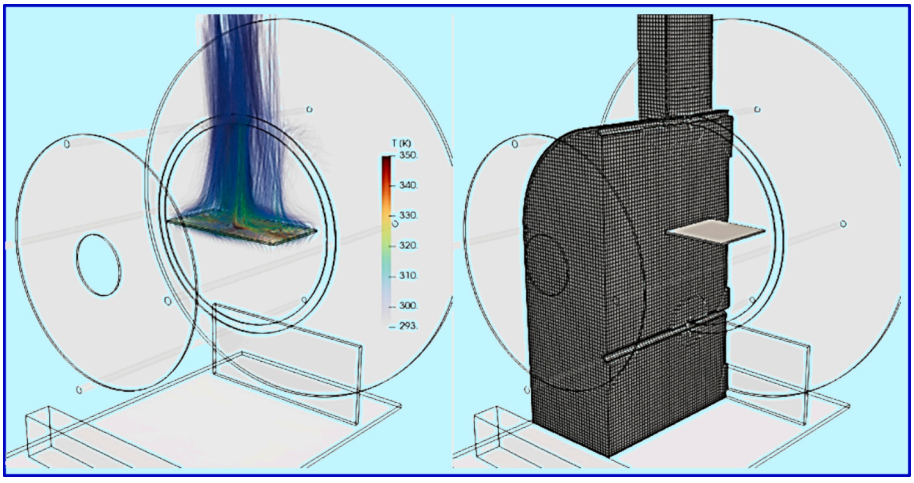

Fig. 5. Example results for case b from Table 2 (left) and discretisation of the flow domain (right).

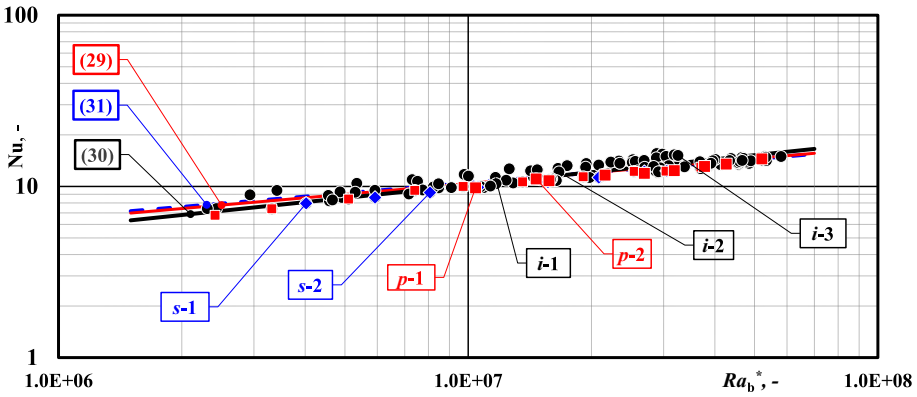

Fig. 6. Experimental results of free convection from a horizontal plate heated on both sides with the same heat flux (CHF). The results of calculations for points *s*, *p* and *i* are listed in Table 1.

Table 1
Documentation of the tests carried out and the work-up of the results, as exemplified by seven randomly selected test points from two series of measurements.

Parameters	Unit	Point names compatible with Fig. 4						
		p-1	*p*-2	*s*-1	*s*-2	*i*-1	*i*-2	*i*-3
$N=U_{up}I_{up} + U_{low}\,I_{up}$	W	2.7014	3.7145	1.0987	2.1240	5.7600	8.7000	26.505
Q_{rad} (23)	W	1.6312	2.1497	0.7108	1.3107	3.3001	4.8971	14.754
Q (22)	W	1.0253	1.4991	0.3717	0.7791	2.3566	3.6432	11.257
$T_{w,av} = (T_{w,up} + T_{w,low})/2$	K	306.70	310.78	299.59	303.55	314.82	324.77	376.51
$T_{\infty,av} = (\sum T_{\infty 1,2,3})/3$	^{0}C	20.17	20.37	20.40	20.40	15.03	13.83	16.23
$T_{av} = (T_{w,av} + T_{\infty})/2$	K	300.01	302.15	296.57	298.98	301.50	305.88	332.95
$\Delta T = T_{w,av} - T_{\infty,av}$	K	13.83	17.26	6.04	10.87	26.64	37.79	86.12
β (17)	1/K	$3.33{\cdot}10^{-3}$	$3.31{\cdot}10^{-3}$	$3.37{\cdot}10^{-3}$	$3.34{\cdot}10^{-3}$	$3.32{\cdot}10^{-3}$	$3.27{\cdot}10^{-3}$	$3.00{\cdot}10^{-3}$
$\nu = \mu/\rho$ (18) and (20)	m^2/s	$1.58{\cdot}10^{-5}$	$1.60{\cdot}10^{-5}$	$1.55{\cdot}10^{-5}$	$1.57{\cdot}10^{-5}$	$1.59{\cdot}10^{-5}$	$1.63{\cdot}10^{-5}$	$1.90{\cdot}10^{-5}$
λ (19)	W/(m·K)	0.02604	0.02620	0.02579	0.02597	0.02615	0.02647	0.02841
$a = \lambda/(c_p\,\rho)$ (18), (19), (21)	m^2/s	$2.20{\cdot}10^{-5}$	$2.23{\cdot}10^{-5}$	$2.15{\cdot}10^{-5}$	$2.19{\cdot}10^{-5}$	$2.22{\cdot}10^{-5}$	$2.28{\cdot}10^{-5}$	$2.66{\cdot}10^{-5}$
$Nu = Nu_{total}$ (15)	–	9.80	11.05	7.95	9.20	11.28	12.14	15.16
Ra (3)	–	$5.31{\cdot}10^{5}$	$6.63{\cdot}10^{5}$	$2.53{\cdot}10^{5}$	$4.38{\cdot}10^{5}$	$1.03{\cdot}10^{6}$	$1.37{\cdot}10^{6}$	$2.14{\cdot}10^{6}$
$Ra^* = Nu{\cdot}Ra$ (16)	–	$1.04{\cdot}10^{7}$	$1.47{\cdot}10^{7}$	$6.06{\cdot}10^{6}$	$8.07{\cdot}10^{6}$	$1.17{\cdot}10^{7}$	$1.67{\cdot}10^{7}$	$3.25{\cdot}10^{7}$
$C^* = Nu/Ra^{*\,0.2}$	–	0.387	0.407	0.380	0.382	0.435	0.436	0.477

in Fig. 6, the following Nusselt - Rayleigh relationships could be derived:

$$Nu = 0.3566{\cdot}Ra^{*0.2092} \quad R^2 = 0.8651 \tag{29}$$

or

$$Nu = 0.181{\cdot}Ra^{*0.25} \tag{30}$$

and

$$Nu = 0.417{\cdot}Ra^{*0.2} \tag{31}$$

where the subscript 'total' has been omitted in the Nusselt figures of Table 1, as well as in Fig. 6.

The experimental tests could only be carried out in practice by setting and maintaining the same heating power of the upper and lower surfaces for each experimental point, i.e. for the CHF condition.

In order to determine more precisely CHF condition it was decided to carry out additional numerical studies.

4.2. Results of the numerical calculations

Example results of the numerical calculations carried out in the form of heat transfer rates Q, which are the averages of the local values $q = Q/A$ obtained for the average values T_w obtained for the condition q = const., are listed in Table 2; all the results are shown in Fig. 7.

Table 2 shows the results of the numerical calculations carried out for six points representing CHF convective heat transfer regime. It also shows the temperatures $T_{total} = (T_{w,up} + T_{w,low})/2$ obtained for the given heat transfer rates Q_{total}. From these calculated values, the Nusselt-Rayleigh relations were determined for each of the cases studied, according to the procedure given in Table 2. The following relationships were obtained for the

$$Nu = 0.7801 \cdot Ra^{*0.1677} \; R^2 = 0.996 \tag{32}$$

or

$$Nu = 0.210 \cdot Ra^{*0.25} \tag{33}$$

and

$$Nu = 0.468 \cdot Ra^{*0.2} \tag{34}$$

4.3. Comparison of the experimental results and numerical calculations

Comparative analysis of the experimental results obtained and the numerical calculations, despite some differences, clearly shows their convergence. This is no coincidence, but a coherent and logical set of results, from which the following preliminary conclusions can be drawn:

- a horizontal plate heated on both sides exchanges heat convectively with the air in the laminar region ($1.3 \cdot 10^6 < Ra^* < 7.8 \cdot 10^7$),
- the lower limits of these ranges, determined by experimental and numerical investigations, are close to each other, while the upper limits, according to numerical calculations, do not exceed $<Ra^* = 2.1 \cdot 10^7$,
- comparison of the experimental results (30) with the numerical ones (33) and (31) with (34) shows that they are well correlated, as their discrepancy is only 13.8 and 10.9% (see Table 4). This tentatively suggests that this convective heat transfer condition can be used to describe the experimental and numerical results obtained with the Type II double-sided heated plate used in this study.

However, before attempting to draw any definitive conclusions about the plausibility of the results of this study and comparison of convective heat transfer from single-sided heated plates, it was decided to verify them against the results of other researchers who almost exclusively studied such plates.

Table 2
Results of the numerical calculations with their scientific work-up in the form of the Nusselt-Rayleigh relationship exemplified by three selected experimental points a, b and c from Fig. 7.

Parameters	Unit	a	b	c
$Q_{total} = Q_{up} + Q_{low}$	W	1.0*	5.0*	12.0*
$T_{w,up} = T_{w,low}$	K	306.20	342.79	394.64
T_∞ setpoint	K	293.15	293.15	293.15
$T_{av} = (T_w\text{-}T_\infty)/2$	K	299.68	317.97	343.90
$\Delta T = T_w\text{-}T_\infty$	K	13.05	49.64	101.49
β (17)	1/K	$3.337 \cdot 10^{-3}$	$3.145 \cdot 10^{-3}$	$2.908 \cdot 10^{-3}$
$\nu = \mu/\rho$ (18), (20)	m^2/s	$1.196 \cdot 10^{-5}$	$2.447 \cdot 10^{-5}$	$2.819 \cdot 10^{-5}$
λ (19)	W/(m·K)	0.02602	0.02734	0.02918
$a = \lambda/(c_p\,\rho)$ (21)	m^2/s	$2.196 \cdot 10^{-5}$	$2.447 \cdot 10^{-5}$	$2.819 \cdot 10^{-5}$
Nu (15)	–	9.82	12.28	13.50
Ra^* (16)	–	$3.668 \cdot 10^6$	$1325 \cdot 10^7$	$2075 \cdot 10^7$
$C^* = Nu/Ra^{*\,0.2}$	–	0.478	0.462	0.465

(*) the setpoints for $Q_{up}/2 = Q_{low}/2$ are marked. (**) T_w is the average surface temperature.

5. Verification and discussion of the results

5.1. Review of the literature on free laminar convective heat transfer

Since convective heat transfer from a horizontal plate heated on both sides (Type II) is no longer a homogeneous phenomenon, unlike convection from the same plate in a vertical position, its comparison with the results of tests on horizontal surfaces with the heating surface facing upwards or downwards does not substantially meet the criterion of correct verification. These two different mechanisms of convective heat transfer were carried out separately on a type I plate heated on one side. In the case of a vertical plate, if the convective heat transfer mechanism is homogeneous and symmetrical, the results depend on its measurement accuracy rather than on the type of plate (I or II) [1].

In this situation, in order to verify the results of the tests carried out, it was decided to choose the relations developed by other authors for the complex cases of free convection, mainly from cuboids, cylinders and spheres. In their case, too, there are surfaces with the heating side facing downwards and upwards, the transformation of which is stepwise (cuboids, vertical cylinders) or smooth (horizontal cylinders, spheres).

The results of the literature review on convective heat transfer from objects with complex heating surface shapes or configurations are given in Table 3 and in Fig. 8.

5.2. Procedure for determining the average correlation

The results of the literature studies worked up in the form of the Nusselt-Rayleigh relationship and summarised in Table 3 were compared qualitatively with the results of the studies carried out in this work. Although they fall within the scope of other authors' research, this is only a subjective comparison. For quantitative verification, the results given in the tables were subjected to optimisation averaging to the form of the average literature relationship for each MLC case.

The MLC values obtained are the result of optimisation involving the simultaneous minimisation of the distance (errors) of the mean correlation from all the f_i correlations from the individual cases in the Table 3.

The method for the optimal choice of the constant C and the exponent n is to mini-mise the

$$\min_{(C,n)\in\Omega} f(C,n) \tag{35}$$

of the error function f, which is defined as follows

$$f(C,n) = \sum_i \sum_j \left| C \bullet Ra_j^n - f_i(C,n) \right| \tag{36}$$

whereby the following constraints are imposed on the independent variables C and n

$$\Omega = \left\{ (C,n) \in \mathbb{R}^2 : 0.1 \le C \le 1.3\,, 0.15 \le n \le 0.3 \right\} \tag{37}$$

The above optimisation problem was discretised so that the f_i correlations from Table 3 are compared for ten evenly distributed Ra_j numbers from the range $10^4 \leqslant Ra_j \leqslant 10^8$.

Among the many optimisation algorithms [42], global optimisation algorithms deserve special attention. They are classified as biologically-inspired metaheuristic or multipoint, derivative-free algorithms. One of the best performing and state-of-the-art global optimisation algorithms [43] is Differential Evolution (DE) [44]. The most popular DE variant – DE/Rand/1/Bin – was chosen to minimise the error function f. A uniform random initial population within the search space was considered. The scale parameter of DE and the crossover probability were 0.7 and

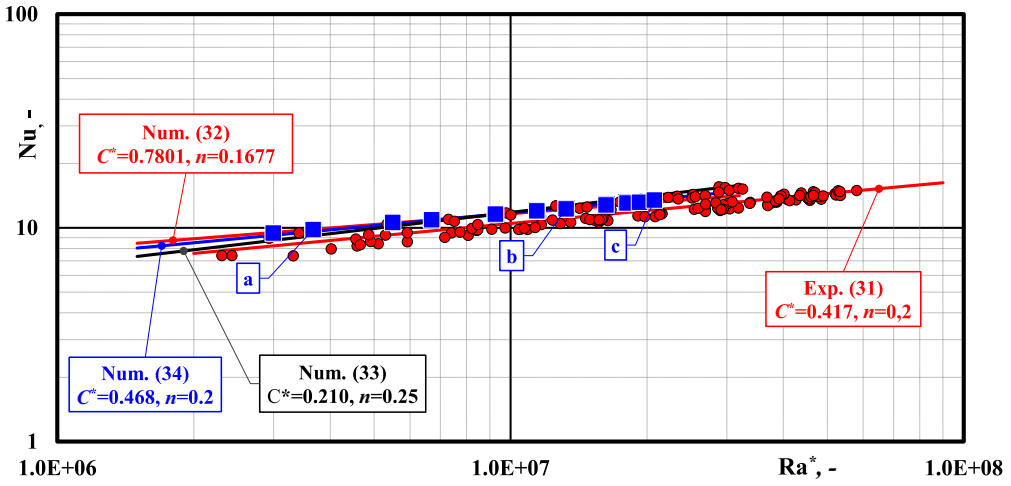

Fig. 7. Results of numerical calculations of convective heat transfer from both sides of a heated horizontal plate according to the CHF regime (blue squares) compared with experimental results (red circles). The numbers indicate the points described in more detail in Table 2. (For interpretation of the references to colour in this figure legend, the reader is referred to the web version of this article.)

Table 3
A compilation of literature data on the results of free convection studies from bodies of different shapes in air.

Equation	Meth.	Range	Additional information	Source	
$Nu = 0.631 \cdot Ra^{*1/6}$ (total) ($Nu = 0.608 \cdot Ra^{*1/6}$ (up). $Nu = 0.654 \cdot Ra^{*1/6}$(lower))	Num.	$9.1 \cdot 10^5 < Ra^* < 1.9 \cdot 10^8$	Horizontal thin plate type II of width *b*: 5.1, 10.2, 20.4, 40.8 and 102 mm, thickness *h* = 0.1, 0.2, 0.4, 0.8 and 2.0 mm.	Chambers, Lee [7]	
$Nu = 1.07 \cdot Ra^{*1/6}$ or $Nu = 1.08 \cdot Ra^{*0.2}$	Exp.	$2.7 \cdot 10^6 \leq Ra^* \leq 2.3 \cdot 10^7$	Horizontal plate, *b* = 76.2 mm, *l* = 254 mm, air	Sparrow, Carlson [12]	
$= Nu_L$ $0.164 \cdot Ra_L^{*\,0.32}$	Exp.	$5 \cdot 10^6 < Ra^* < 5 \cdot 10^8$	Rectangular plates *L* = 305, 508 mm, water, horizontal	King [11]	a
$= Nu_x$ $0.563 \cdot Ra_x^{*\,0.199}$		$3 \cdot 10^5 < Ra^* < 6.3 \cdot 10^{12}$	vertical,		b
$= Nu_D$ $0.800 \cdot Ra_D^{*\,0.175}$	Num.	$1 < Ra^*_D < 10^7$	Horizontal cylinder, air	Qureshi, [14]	
	Exp.	$2 \cdot 10^6 < Ra^*_D < 6.3 \cdot 10^6$	*D* = 43.75 mm, *L* = 375 mm		
$Nu_D = 0.744 \cdot Ra_D^{*\,0.25}$	Exp.	$10^4 < Ra^*_D < 1 \cdot 10^8$	Horizontal cylinder, air	Churchill [15]	
$Nu_D = 0.6 \cdot Ra_D^{*\,0.2}$	Exp.	$3 \cdot 10^8 < Ra^*_D < 2.5 \cdot 10^{10}$	Horizontal cylinder, water	Kitamura et al. [21]	
$Nu_D = 0.47 \cdot Ra_D^{*0.2}$	Exp.	$1.1 \cdot 10^7 < Ra^*_D < 8 \cdot 10^7$	60 ≤ D ≤ 800 mm, Elliptic horizontal tube: *L* = 1 m *D* = 90 mm, *d* = 50 mm, water	Ali [32],	

0.9 respectively. The algorithms terminated when 40 generations were reached. Moreover, the population size was set to 30. The results of the global optimisation literature relations collected in Table 3 and graphically shown in Fig. 8 are listed below:

$$Nu = 0.56356 \cdot Ra^{*0.198944} \quad (38)$$

MLC in Fig. 8,

$$Nu = 0.256 \cdot Ra^{*0.25} \quad (39)$$

valid for the experimental and numerical range $6 \cdot 10^5 \leq Ra \leq 6 \cdot 10^7$ (accuracy −10.40% ≤ Nu ≤13.35%),

$$Nu = 0.554 \cdot Ra^{*0.2} \quad (40)$$

valid for the experimental and numerical range $6 \cdot 10^5 \leq Ra \leq 6 \cdot 10^7$ (accuracy −0.31% ≤ Nu ≤0.18%).

5.3. Comparison of the literature, experimental and numerical results

The reason for converting the average correlations of the MLC literature data (38) into equivalent correlations, but with the given exponent $n = 1/4$ or $n = 1/5$ (39) and (40), was to verify the correctness of the experimental and numerical correlations, which were also described with the same exponents. A comparison of the experimental and numerical correlations with the literature using different *C* constants and *n* exponents would have been possible but would have been cumbersome and difficult to interpret.

Since the correlations $MLC_{n=1/4}$ and $MLC_{n=1/5}$ differ slightly within the narrow range of this study, the divergence errors are naturally comparable (see Table 4). An additional advantage of working with two exponents in parallel is that the results are comparable not only with the averages but also with the individual correlations of each author (see Tables 2 and 3).

The results of the divergence of the correlations obtained experimentally and numerically with the averaged MLC literature values are summarised in Table 4.

5.4. Discussion

The analysis of the discrepancies in the results listed in Table 4 shows that the double-sided heated Type II plate tested in the experiments satisfies the CHF convective heat transfer condition. This is confirmed both by the slight deviations from the numerical calculation results of −10.9% for $n = 1/5$ and − 13.8% for $n = 1/4$ and by the −24.7% ($n = 1/5$) and − 29.3% ($n = 1/4$) averaged deviations from the results of other researchers (MLC), who investigated both single-sided heated plates and solids with multiple heat transfer surfaces.

The average of the first two values, i.e. -12.4% is almost half that of the average of the other two values, i.e. -27%, which is due to the fact that the numerical calculations reproduce exactly the same double-sided heated plate (Type II), the actual dimensions of the plate and the test bench as well as the thermodynamic conditions of the experiments carried out. The averaged MLC relationships of other researchers were

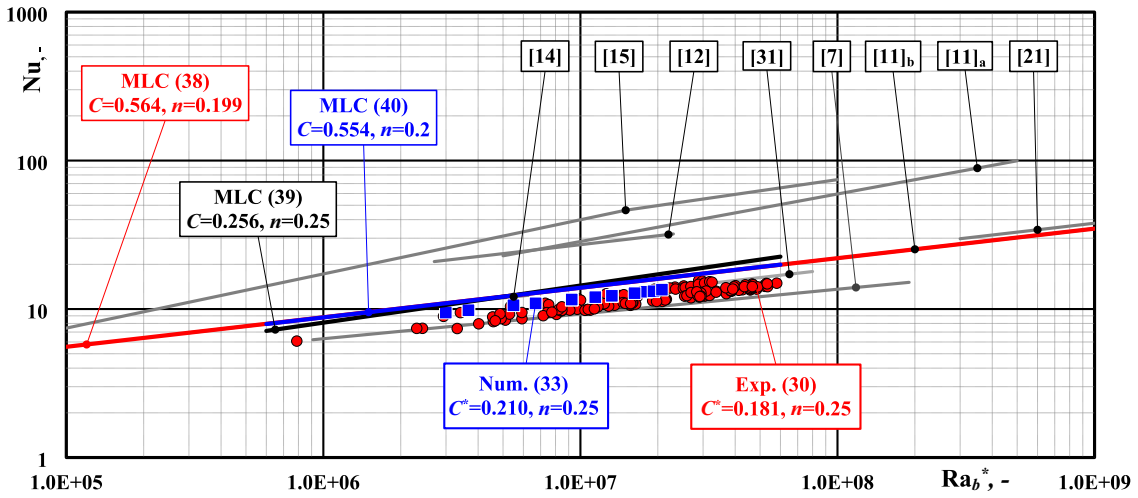

Fig. 8. Comparison of the experimental (red circles) and numerical (blue squares) results of convective heat transfer from a horizontal plate heated on both sides with the results from objects of different shapes by other authors, approximated by the least squares fit (red line) mean correlations (MLC) or for a forced slope: $n = 1/4$ (black line) and $n = 1/5$ (blue line). (For interpretation of the references to colour in this figure legend, the reader is referred to the web version of this article.)

Table 4
Comparison of experimental results, numerical calculations and literature averages MLC expressed in the form of Nusselt-Rayleigh relations with $n = 1/4$ and $n = 1/5$ for the CHF condition.

CHF		Exp.		Num.	
		(30) $n = 1/4$ $C^* = 0.181$	(31) $n = 1/5$ $C^* = 0.417$	(33) $n = 1/4$ $C^* = 0.210$	(34) $n = 1/5$ $C^* = 0.468$
MLC	(39) $C^* = 0.256$, $n = 1/4$	−29.3%	–	−18.0%	–
	(40) $C^* = 0.554$, $n = 1/5$	–	−24.7%	–	−15.5%
Num.	(33) $C^* = 0.210$, $n = 1/4$	−13.8%	–	–	–
	(34) $C^* = 0.468$, $n = 1/5$	–	−10.9%	–	–

obtained for convective heat transfer from unilaterally heated plates (Type I) and from three-dimensional heating elements. In addition, these researchers used benches of different dimensions and used different test procedures.

At this point, it should also be emphasized that the research carried out was not devoted to exploring the phenomena of free convection occurring during simultaneous heat transfer from the top and bottom horizontal surfaces, together with their interaction. The aim of the research was only to test the tool necessary to carry out this type of research, i.e. the correctness of the operation and the sufficiently high accuracy of the results of a double-sided heated plate (Type II).

In summary, the typical divergence between the experimental and numerical results shows that the convective heat transfer in air from a horizontal double-heated constant heat flux plate Type II in the laminar range has been clearly and positively verified.

The slightly larger discrepancies with the MLC, the reasons for which have been explained above, do not undermine this thesis, but suggest that there are differences in heat transfer between Type I and Type II plates which require further investigation.

6. Conclusions

The aim of this research was to develop and test a tool for studying convective heat transfer in air using the balance method, which is not a very accurate method owing to the problems involved in estimating heat loss and thus determining the actual value of convective heat flux. For this purpose, a novel version of the horizontal heating plate was designed and assembled.

By minimizing heat loss from the sides of the plate, their design significantly improved the accuracy of heat transfer studies using the balance method. This is because the convective heat transfer from a double-sided heated plate resembles the heat transfer from a cuboid (solid) than from a single-sided heated plate (surface).

The experimental results of convective heat transfer from a horizontal double-heated plate to air led to the development of a relationship: $Nu = 0.3566 \cdot Ra^* 0.2092$ for CHF condition, and it is valid in the Rayleigh number range $6.105 < Ra^* < 6.107$, i.e. for the laminar range. Approximated by Eqs. (30) and (33) for $n = 1/4$ and by (31) and (34) for $n = 1/5$, the good correlation of these relations with the numerical solution, i.e. -12.4% (mean error for $n = 1/4$ and $n = 1/5$), and a slightly inferior correlation with the results of other researchers, i.e. -27.0%, provide evidence for the positive verification of this heat transfer study using a Type II plate.

The experimental investigations carried out in this research, and the compatibility of the results obtained with numerical calculations and literature data, open up new possibilities for studying free convection not only from a horizontal plate as a whole, but also from its upper and lower surfaces, treated separately and with their interactions.

CRediT authorship contribution statement

Michał Ryms: Writing – review & editing, Writing – original draft, Methodology, Investigation, Data curation, Conceptualization. **Krzysztof Tesch:** Writing – original draft, Validation, Software, Conceptualization. **Witold s.M. Lewandowski:** Writing – review & editing, Writing – original draft, Visualization, Validation, Supervision, Conceptualization.

Declaration of competing interest

The authors declare that they have no known competing financial interests or personal relationships that could have appeared to influence the work reported in this paper.

Data availability

Data will be made available on request.

References

[1] M. Ryms, W.M. Lewandowski, Evaluating the influence of radiative heat flux on convective heat transfer from a vertical plate in air using an improved heating plate, Int. J. Heat Mass Transf. 173 (2021) 121232, https://doi.org/10.1016/j.ijheatmasstransfer.2021.121232.

[2] M. Ryms, G.J. Kwiatkowski, W.M. Lewandowski, On the differential effect of temperature on the Nusselt-Rayleigh relationship in free convection, Int. J. Therm. Sci. 181 (2022) 107744, https://doi.org/10.1016/j.ijthermalsci.2022.107744.

[3] W.W. Yousef, J.D. Tarasuk, W.J. Mckeen, Free convection heat transfer from upward-facing isothermal horizontal surface, ASME Trans. J. Heat Transf. 104 (1982) 493–500.

[4] M. Al-Arabi, M.K. Al-Riedy, Natural convection heat transfer from isothermal plate of different shapes, Int. J. Heat Mass Transf. 19 (1976) 1399–1404.

[5] Khalifa N. Abdul-Jabbar, Natural convective heat transfer coefficient - a review, I. Isolated vertical and horizontal surfaces, Energy Convers. Manag. 42 (2001) 491–504.

[6] C.J. Kobus, G.L. Wedekind, An experimental investigation into natural convection heat transfer from horizontal isothermal circular disks, Int. J. Heat Mass Transf. 44 (17) (2001) 3381–3384, https://doi.org/10.1016/s0017-9310(00)00330-6.

[7] B. Chambers, T.Y.T. Lee, A numerical study of local and average natural convection Nusselt numbers for simultaneous convection above and below a uniformly heated horizontal thin plate, J. Heat Transf. 119 (1) (1997) 102–108, https://doi.org/10.1115/1.2824074.

[8] A. Jaffer, Natural convection heat transfer from an isothermal plate, Thermo 3 (2023) 148–175, https://doi.org/10.3390/thermo3010010.

[9] A. Kalendar, et al., Natural convective heat transfer from horizontal isothermal surface of polygons of octagonal and hexagonal shapes, J. Therm. Sci. Eng. Appl. 11 (5) (2019) 1–44, https://doi.org/10.1115/1.4043006.

[10] Y. Fan, Y. Zhao, J.F. Torres, F. Xu, Ch. Lei, Y. Li, J. Carmeliet, Natural convection over vertical and horizontal heated flat surfaces: a review of recent progress focusing on underpinnings and implications for heat transfer and environmental applications, Phys. Fluids 33 (2021) 101301, https://doi.org/10.1063/5.0065125.

[11] J.A. King, Natural Convection above Heated Inclined Surfaces, Ph.D. Dissertation, Louisiana State University, Baton Rouge, Louisiana, 1989, p. 212, https://doi.org/10.31390/gradschool_disstheses.4854.

[12] E.M. Sparrow, C.K. Carlson, Local and average natural convection Nusselt numbers for a uniformly heated, shrouded or unshrouded horizontal plate, Int. J. Heat Mass Transf. 29 (3) (1986) 369–379, https://doi.org/10.1016/0017-9310(86)90207-3.

[13] M. Eslami, K. Jafarpur, Laminar natural convection heat transfer from isothermal cylinders with active ends, Heat Transf. Eng. 32 (6) (2011) 506–513, https://doi.org/10.1080/01457632.2010.506378.

[14] Z.H. Qureshi, R. Ahmad, Natural convection from a uniform heat flux horizontal cylinder at moderate Rayleigh numbers, Numer. Heat Transf. 11 (2) (1987) 199–212, https://doi.org/10.1080/10407788708913550.

[15] S.W. Churchill, H.H.S. Chu, Correlating equations for laminar and turbulent free convection from a horizontal cylinder, Int. J. Heat Mass Transf. 18 (1975) 1049–1053, https://doi.org/10.1016/0017-9310(75)90222-7.

[16] V.T. Morgan, The overall convective heat transfer from smooth circular cylinders, Adv. Heat Tran. 11 (1975) 199–264, https://doi.org/10.1016/s0065-2717(08)70075-3.

[17] S.K.S. Boetcher, Natural Convection from Circular Cylinders, Springer Cham Heidelberg New York Dordrecht London, 2014, https://doi.org/10.1007/978-3-319-08132-8.

[18] K. Jodlbauer, Das Tcmperatur- und Geschwindigkeitsfeld um ein geheiztes Rohr bei freier Konvektion, Forsch. Geb. Ingenieurw. 4 (1933) 157–172.

[19] G. Etemad, Free convection heat transfer from a rotating horizontal cylinder to ambient air with interferometric study of flow, Trans. ASME 77 (1955) 1283–1289.

[20] F. Wamsler, Die Wärmeabgabe geheizter Körper an Luft, Ver Deut Ing Forschunash 98/99 (1911).

[21] K. Kitamura, F. Kami-iwa, T. Misumi, Heat transfer and fluid fow of natural convection around large horizontal cylinders, Int. J. Heat Mass Transf. 42 (1999) 4093–4106, https://doi.org/10.1016/S0017-9310(99)00079-4.

[22] S.M.H. Jayhooni, K. Jafarpur, Numerical simulation of laminar free convection heat transfer around isothermal concave and convex body shapes, J. Heat Mass Transf. Res. 2 (2015) 37–44. http://jhmtr.journals.semnan.ac.ir.

[23] M.M. Yovanovich, K. Jafarpur, Models of laminar natural convection from vertical and horizontal isothermal cuboids for all Prandtl numbers and all Rayleigh numbers below 10^{11}, and ASME, Fundam. Nat. Convect. HTD 26 (1993) 111–126.

[24] J.R. Culham, M.M. Yovanovich, P. Teertstra, C.-S. Wang, Simplified analytical models for forced convection heat transfer from cuboids of arbitrary shape, EEP-Vol. 26-1, Adv. Electron. Pack. ASME 1 (1999) 105–113, https://doi.org/10.1115/1.1347993.

[25] E. Radziemska, W.M. Lewandowski, Natural convective heat transfer from isothermal cuboids, Int. J. Heat Mass Transf. 46 (2003) 2169–2178, https://doi.org/10.1016/S0017-9310(02)00533-1.

[26] J.R. Culham, M.M. Yovanovich, P. Teertstra, C.-S. Wang, G. Refai-Ahmed, R.-M. Tain, Simplified analytical models for forced convection heat transfer from cuboids of arbitrary shape, J. Electron. Packag. 123 (3) (2001) 182–188, https://doi.org/10.1115/1.1347993.

[27] E. Radziemska, W.M. Lewandowski, Experimental verification of natural convective heat transfer phenomenon from isothermal cuboids, Exp. Thermal Fluid Sci. 32 (2008) 1034–1038, https://doi.org/10.1016/j.expthermflusci.2007.11.001.

[28] S.W. Churchill, R.U. Churchill, A comprehensive correlating equation for heat and component transfer by free convection, AICHE J. 21 (1975) 604–606, https://doi.org/10.1002/aic.690210330.

[29] J.R. Culham, M.M. Yovanovich, S. Lee, Thermal modeling of isothermal cuboids and rectangular heat sinks cooled by natural convection, IEEE Trans. Components Pack. Manufact. Technol. Part A 18 (3) (September 1995) 559–566.

[30] D.J. Cha, S.S. Cha, Three-dimensional natural convection flow around two interacting isothermal cubes, Int. J. Heat Mass Transf. 38 (13) (1995) 2343–2352, https://doi.org/10.1016/0017-9310(94)00359-4.

[31] M.M. Yovanovich, Natural convection from isothermal convex bodies - Simple models for bounds on body - gravity function, AIAA-2000-2581, 2024, https://doi.org/10.2514/6.2000-2581.

[32] M. Ali, S. Sadek, Free convection heat transfer from different objects, Heat Transf. (2018), https://doi.org/10.5772/intechopen.75427.

[33] S. Lee, M.M. Yovanovich, K. Jafarpur, Effects of geometry and orientation on laminar natural convection from isothermal bodies, J. Thermophys. Heat Transf. 5 (1991) 208–216, https://doi.org/10.2514/3.249.

[34] A.O. Elsayed, E.Z. Ibrahim, S.A. Elsayed, Free from a constant heat flux elliptic tube, Energy Convers. Manag. 44 (2003) 2445–2453, https://doi.org/10.1016/S0196-8904(03)00002-5.

[35] L. Boukhattem, H. Hamdi, D.R. Rousse, Numerical simulation of heat transfers in a room in the presence of a thin horizontal heated plate, Energy Procedia 42 (2013) 549–556, https://doi.org/10.1016/j.egypro.2013.11.056.

[36] Y. Jiang, B. Nie, F. Xu, Lapping flow and starting plume on an evenly heated horizontal plate, Int. J. Heat Mass Transf. 138 (2019) 235–243. https://www.x-mol.net/paper/article/5648272.

[37] Y. Jiang, B. Nie, Zhao, et al., Scaling of buoyancy-driven flows on a horizontal plate subject to a ramp heating of a finite time, Int. J. Heat Mass Transf. 171 (2021) 121061, https://doi.org/10.1016/j.ijheatmasstransfer.2021.121061.

[38] J.J. Wei, B. Yu, Y. Kawaguchi, Simultaneous natural-convection heat transfer above and below an isothermal horizontal thin plate, Numer. Heat Transf. Part A 44 (2003) 39–58.

[39] R. Manna, Natural Convective Heat Transfer from Horizontal and Inclined Two-Sided Bodies of Finite Thickness, Ph.D. Dissertation, Queen's University Kingston, Ontario, Canada October, 2019, pp. 1–231, http://hdl.handle.net/1974/26706.

[40] OpenFOAM. https://www.openfoam.com, 2024.

[41] R.I. Issa, Solution of the implicitly discretized fluid flow equations by operator-splitting, J. Comput. Phys. 62 (1986) 40–65, https://doi.org/10.1016/0021-9991(86)90099-9.

[42] K. Tesch, Continuous Optimisation Algorithms, Gdańsk University of Technology Publishers, Gdańsk, 2016. https://pbc.gda.pl/dlibra/publication/65394/edition/58843/content.

[43] K. Tesch, K. Kaczorowska, Arterial cannula shape optimization by means of the rotational firefly algorithm, Eng. Optim. 48 (3) (2016), https://doi.org/10.1080/0305215X.2015.1018677.

[44] R. Storn, K. Price, Differential evolution - a simple and efficient heuristic for global optimization over continuous spaces, J. Glob. Optim. 11 (4) (1997) 341–359, https://doi.org/10.1023/A:1008202821328.

Nomenclature

Symbols

a: coefficient of thermal diffusivity, m^2/s
A: surface area, m^2
b: width, m
B: width, thickness, m
c_p: specific heat, J/(kg·K)
C: coefficient in the Rayleigh–Nusselt equation, (1)
CFD: Calculation Fluid Dynamic
CHF: Constant Heat Flux of the plate
CWT: Constant Wall Temperature
d: diameter of the wire, mm
D: diameter of circle plate, m
DE: Differential Evolution
DILU: Diagonal-based Incomplete Lower Upper
f: error function
F: cross-section, m^2
F(Pr): Prandtl number function
g: acceleration due to gravity, m/s^2
g: thickness, mm
G: component values of the body-gravity function [1]
GAMG: Generalised geometric-Algebraic Multi-Grid
h: height, thickness of the plate, m
H: height, m
I: current, A
I/O: Inlet/Outlet
l: length, m
L: length, m
LAM100X160H0.6: copper-clad epoxy laminate 0.6 mm thick on one side (H) or on two sides (ED) with dimensions (100x160 mm)
MLC: mean literature correlation
n: exponent
N: heater power, W

Nu: Nusselt number, dimensionless, (15)
O: perimeter of the plate, m
PISO: Pressure-Implicit with Splitting of Operators
Pr: Prandtl number
R: radius, m
R: resistance, Ω
Ra: Rayleigh number, dimensionless, (3)
Ra:* modified Rayleigh number, dimensionless, (16)
s: width, mm
S: dimensionless shape factor [1], $= b \cdot \sqrt{A}\ /A$
T: temperature, °C, K
q: heat flux, W/A
Q: heat transfer rate, W
U: current voltage, V
UHF: Uniform Heat Flux
y: coordinate
x: coordinate
z: coordinate

Greek letters

α: heat-transfer coefficient, W/(m^2·K)
α: thermal coefficient of resistance, 1/K
β: coefficient of thermal expansion, 1/K
δ: boundary layer thickness, mm
ε: surface emissivity coefficient
σ: Stefan-Boltzmann constant, W/(m^2·K^4)
Δ: difference
λ: thermal conductivity, W/(m·K)
μ: dynamic viscosity, kg/(m·s)
η: moderate length of the plate $= A/O = b \cdot l/(2 \cdot b + 2 \cdot l)$, m
ρ: density, kg/m^3
ρ: specific resistance, Ω·m
ν: kinematic viscosity, m^2/s
τ: time, s

Subscripts

air: in air
av: average
bot: abbreviation for lower (bottom) surface
ch: characteristic
conv: convective
Cu: copper
low: abbreviation for facing downwards
hor: horizontal
loss: heat losses
max: maximum
rad: radiative
t: temperature
top: abbreviation for upper (top) surface
total: overall
up: abbreviation for facing upwards
w: wall
vert: vertical
∞: in surroundings
0: reference temperature